Supporting Information

Active Sites in Single-Atom Fe−N_x−C Nanosheets for Selectively Electrochemical Dechlorination of 1,2-Dichloroethane to Ethylene

Guoqiang Gan†, *Xinyong Li**†, *Liang Wang*†, *Shiying Fan*†, *Jincheng Mu*†, *Penglei Wang*†, *Guohua Chen**‡

† State Key Laboratory of Fine Chemicals, Key Laboratory of Industrial Ecology and Environmental Engineering (MOE), School of Environmental Science and Technology, Dalian University of Technology, Dalian 116024, China

‡Department of Mechanical Engineering, The Hong Kong Polytechnic University, Hung Hom, Kowloon, Hong Kong SAR, China

* Corresponding Author.

E-mail: xyli@dlut.edu.cn；guohua.chen@polyu.edu.hk

1. EXPERIMENTAL METHODS

Chemicals and Materials

Dopamine hydrochloride and $FeCl_3 \cdot 6H_2O$ was purchased from Sinopharm Chemical Reagent Co., Ltd., and other chemicals were purchased from Tianjin Kemiou Chemical Reagent Co., Ltd. All the chemicals were in analytical grade and used as received without further purification.

Characterization

XAS was performed at room temperature on the 1W1B beamline of Beijing Synchrotron Radiation Facility (BSRF), China. The catalysts (~30 mg) were pelletized as disks of 6 mm diameter using paraffin as a binder. Transmissive-mode Fe K-edge X-ray absorption spectra were collected for all samples over a range of 6974−8110 eV, where a 100% Ar filled Lytle ion-chamber detector with Mn X-ray filters and soller slits were used. The monochromator energy was calibrated using a Fe foil. The storage ring of BSRF was working at the energy of 2.5 GeV with a maximum electron current of 250 mA. The hard X-ray was monochromatized with Si (111) double-crystal monochromator, and the detuning was done by 30% to remove harmonics. The acquired EXAFS data were processed according to the standard procedures using the ATHENA module of the IFEFFIT software packages. The k^3-weighted χ (k) data in the *k* space ranging from 2.0 - 12.0 $Å^{-1}$ was Fourier transformed to real (*R*) space using a hanning windows (dk = 1.0 $Å^{-1}$) to separate the EXAFS contributions from different coordination shells. To obtain the detailed structural parameters around Fe atom in the as-prepared samples, the quantitative curve-fittings were carried out for the Fourier transformed $k^3\chi$ (k) in the *R* space using the ARTEMIS module of IFEFFIT3. Fe_6N_2 and Fe_2O_3/FeO were

used to simulate the Fe−N and Fe−O bonds, respectively. Considering the similar bond length of Fe−N and Fe−O bonds, only Fe−N bond was simulated in Fe−N_x−Cns−800. Effective backscattering amplitudes F(k) and phase shifts Φ (k) of all fitting paths were calculated by the *ab initio* code FEFF8.0. To fit the data of samples, the interatomic distance (R) and the Debye-Waller factor (σ^2) were allowed to vary.

High-angle annular dark field scanning transmission electron microscopy (HAADF-STEM), and aberration-corrected TEM were recorded on an FEI Talos F200X. Transmission electron microscopic analysis was performed on a FEI Tecnai G^2 F30 STWIN (USA) instrument equipped with a Schottky field emission gun (FEG), a Super-twin alpha objective lens, and operated at 300 kV accelerating voltage, while the corresponding elemental maps were obtained under the plane scanning mode. Scanning electron microscopy (SEM) were measured on S-3400N (Hitachi, Japan) equipped with an energy dispersive X-ray spectrometer. Atomic force microscopy (AFM) was conducted on Dimension Icon (Bruker, USA) with a force constant of ~ 48 N/m and scanning rate of 1.0 Hz. X-ray diffractometer (XRD) was tested on Rigaku Corporation D/max-2400 with Cu Kα radiation at 30 kV. Perkin-Elmer PHI 5600 electron spectrometer with Al Kα radiation served as X-ray photoelectron spectroscopy (XPS) measurements. Raman was measured on an Invia/Reflrx Lasser Micro-Raman spectroscope (Renishaw, England). The metal loadings of the catalysts were determined with Inductively Coupled Plasma Atomic Emission Spectroscopy (ICP-AES) on an IRIS Intrepid II XSP instrument (Thermo Electron Corp.). Before analysis, a proper amount of powder sample was treated by hot aqua regia to get a clear solution.

Electrochemical measurements

The electrocatalytic dechlorination of DCE was conducted using a three-electrode electrochemical workstation (CHI 760C, Shanghai Chenhua, China) in an undivided cell filled with 50 mL 0.1 M $(C_3H_7)_4NBF_4$ DMF solution, where a Pt plate was performed as counter electrode and an Ag/AgCl/Me_4NCl (sat) in DMF + CH_3CN (3:1, *v*/*v*) as reference electrode. The reference electrode was calibrated at the end of each experiment against the ferrocenium/ferrocene couple (E°_{Fc+}/F_c = 0.475 V *vs* SCE in DMF), and all potentials were referenced to the saturated calomel electrode (SCE) scale. The cyclic voltammograms experiments were performed at a scan rate of 0.1 V s^{-1} with the ranging from −1.0 V to −2.85 V (E *vs* SCE/V). The working electrode comprised of the Fe−N_x−Cns that were brushed on glassy carbon electrodes (GCE, 3 mm in diameter, type L) with catalyst loading of 0.2 mg cm^{-2}, and the concentration of DCE was 0.01 M. The electrolysis experiments were performed under the constant voltage model with 0.10 M DCE, and the carbon cloth with catalyst loading of 1.0 mg cm^{-2} was applied as working electrode.

Analysis

The outlet volatile organic compounds were analyzed using an Agilent GC/MS 6890-5975 system equipped with a HP-5 (30 m × 0.25 mm × 0.25 μm) capillary column (Agilent Technologies, USA). The oven temperature was set at 60 °C and held for 4 min, then increased to 280 °C at the rate of 10 °C min^{-1} and held for 1 min. He with a flow rate of 0.5 mL min^{-1} was used as a carrier gas. The hydrogen was detected quantificationally by external standard method on gas chromatography (Agilent 7890A) equipped with tandem TCD detector, in which Porapak Q and MolSieve 5A chromatographic columns were used to separate the reaction gas

at 50 °C.

The selectivity of ethylene was determined by the following Eq. (S1).

$$\text{Selectivity} = \frac{N\,(\text{ethylene})}{N\,(\text{vinyl chloride})} \qquad \text{(S1)}$$

The FE (%) of ethylene was determined by the following Eq. (S2).

$$\text{FE}\,(\%) = \frac{N\,(\text{ethylene})}{Q\,/(\text{n} \times F)} \times 100\% \qquad \text{(S2)}$$

Where Q is the total charge passed through the electrodes, n is the number of electrons that form a molecule of ethylene, n = 2; F is the Faraday constant.

Theoretical Calculations

The dechlorination process of CH_2ClCH_2Cl into CH_2CH_2 on Fe−N_3 and Fe−N_4 sites was investigated by the Vienna *Ab-initio* Simulation Package (VASP) using the revised Perdew-Burke-Ernzerhof (RPBE) of the generalized gradient approximation (GGA). The interaction between valence electrons and ionic used the PAW pseudo-potential. A carbon layer containing 123 C atoms was used to describe the graphene, which was used to support Fe−N_3 and Fe−N_4 sites. The energy convergence of 1.0×10^{-4} eV and the cutoff energy of 400 eV were adopted to perform the geometry optimization. After geometry optimization, the energy convergence of 1×10^{-5} eV and the Monkhorst-Pack mesh of 4 × 4 × 1 were used to calculate the density of state (DOS) plots of Fe−N_3 and Fe−N_4.

Gibbs free energy changes (ΔG) of all reaction steps are calculated by the known standard hydrogen electrode (SHE) model, which is used to evaluate the reaction barrier. The chemical potential of a proton-electron pair, $\mu\,(H^+) + \mu\,(e^-)$, is equal to the half of the chemical potential of one gaseous hydrogen, $1/2\mu\,(H_2)$, at U = 0 V *vs* SHE at pH = 0.

The mechanism of DCE reduction reaction was considered as shown below

a) $CH_2ClCH_2Cl \xrightarrow[\text{Dechlorination}]{\lightning} \underbrace{CH_2CH_2 + CH_2CHCl}_{> 99\%} + HCl + H_2 + \underbrace{\text{other components}}_{< 1\%}$

$CH_2ClCH_2Cl + e^- + H^+ \rightarrow {}^*CH_2CH_2Cl + HCl$ (1)

${}^*CH_2CH_2Cl + e^- + H^+ \rightarrow CH_2CH_2 + HCl$ (2)

${}^*CH_2CH_2Cl + e^- + H^+ \rightarrow CH_2CHCl + H_2$ (3)

b) $H^+ + e^- \xrightarrow{\lightning} H_2$

Scheme S1. a) Electrocatalytic DCE dechlorination reaction and b) hydrogen evolution reaction at cathode.

2. Additional data

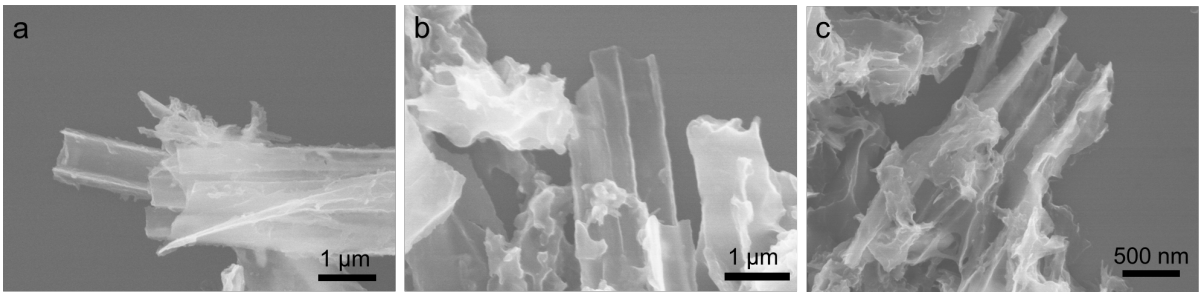

Figure S1. SEM images of a) Fe−N_x−Cns−700, b) Fe−N_x−Cns−800, and c) Fe−N_x−Cns−900.

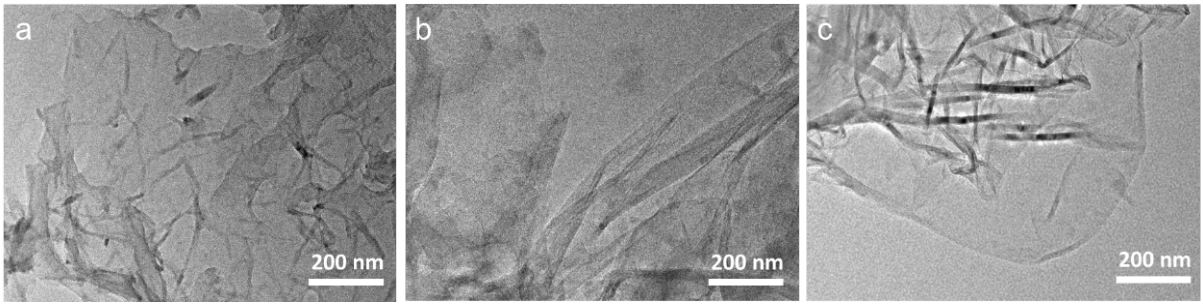

Figure S2. TEM images of a) Fe−N_x−Cns−700, b) Fe−N_x−Cns−800, and c) Fe−N_x−Cns−900.

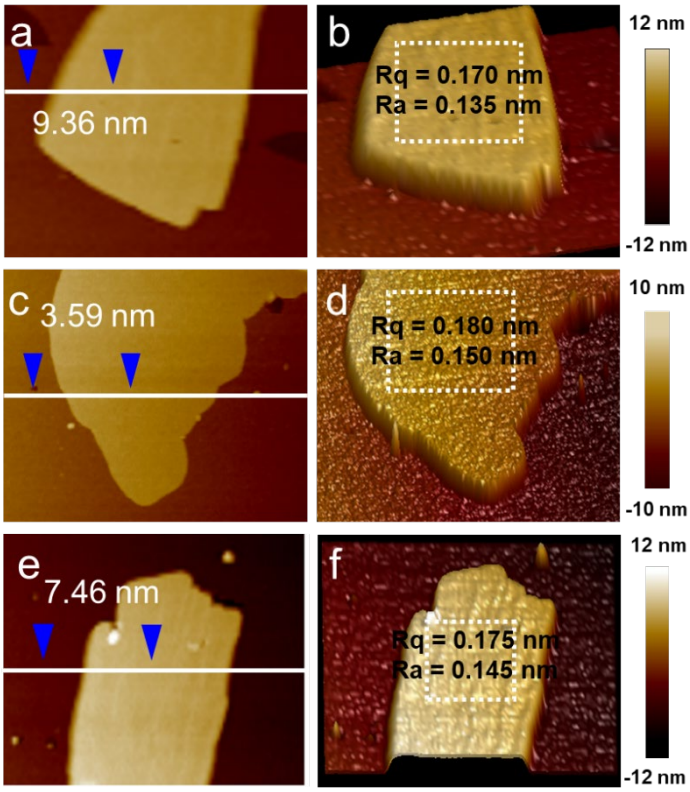

Figure S3. a, c, e) 2D AFM images, and b, d, f) 3D AFM images of Fe−N_x−Cns−700, Fe−N_x−Cns−800 and Fe−N_x−Cns−900.

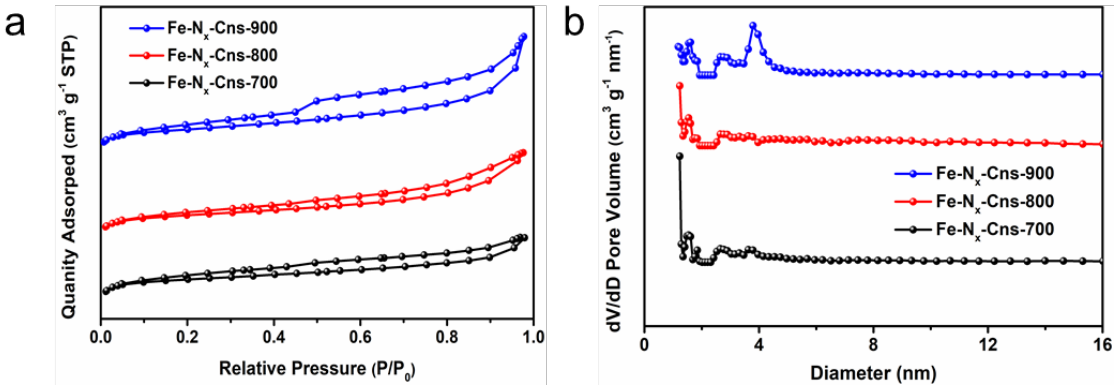

Figure S4. a) N_2 adsorption/desorption isotherms, and b) DFT pore size distribution of Fe−N_x−Cns.

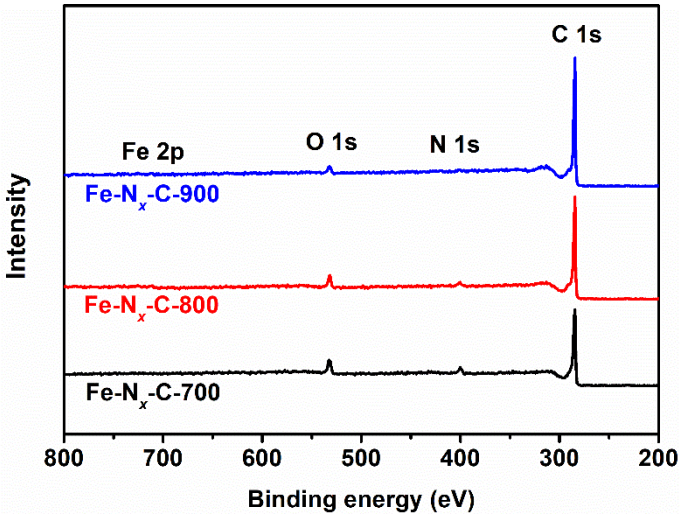

Figure S5. XPS survey spectra of Fe–N_x–Cns.

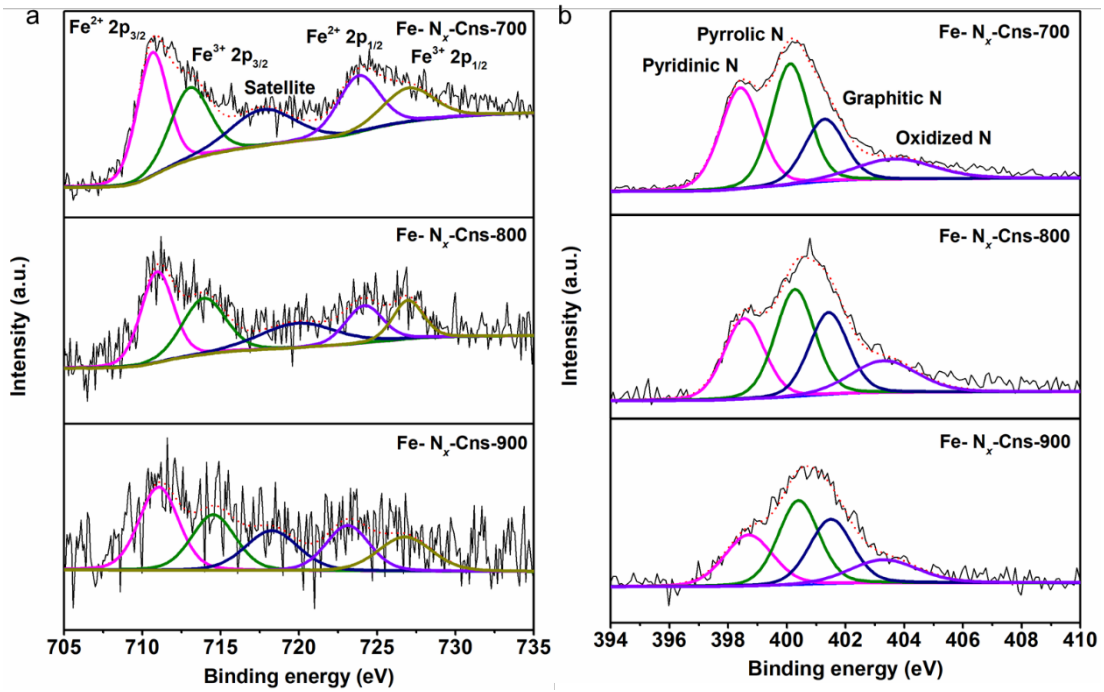

Figure S6. a) Fe 2p XPS spectra, and b) N 1s XPS spectra of Fe−N_x−Cns.

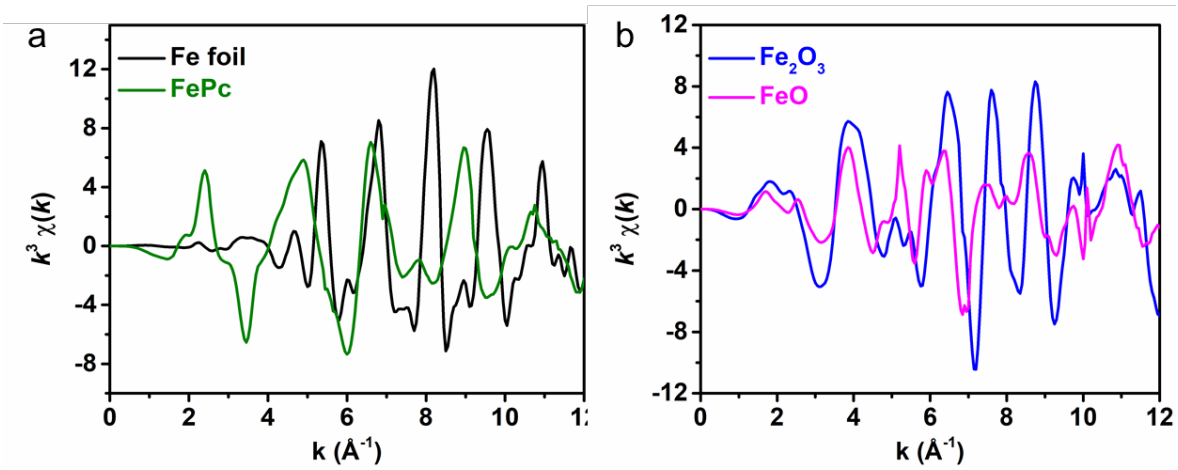

Figure S7. FT-EXAFS analysis of a) Fe foil, FePc, and b) Fe_2O_3, FeO in *k* space.

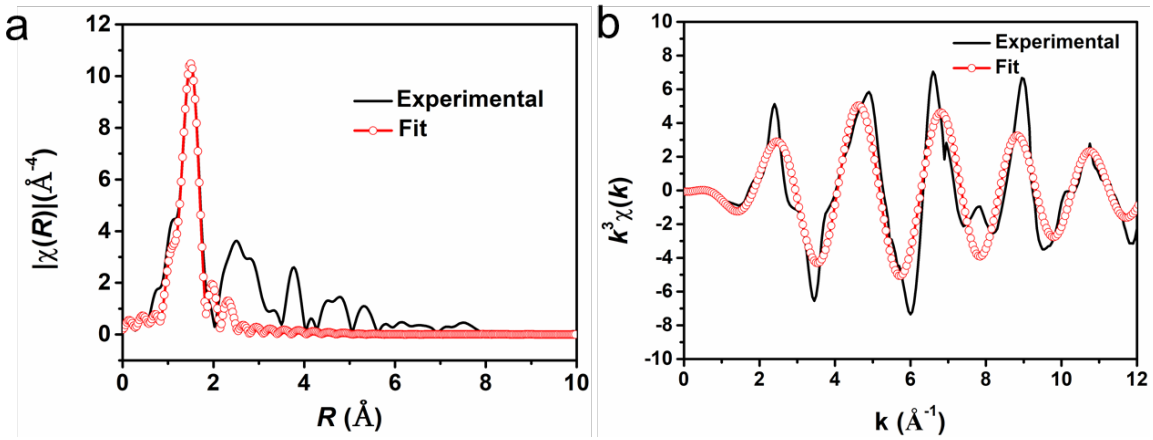

Figure S8. Comparison between experimental and fitting results of FT-EXAFS spectrum in a) *R* and b) *k* space of FePc.

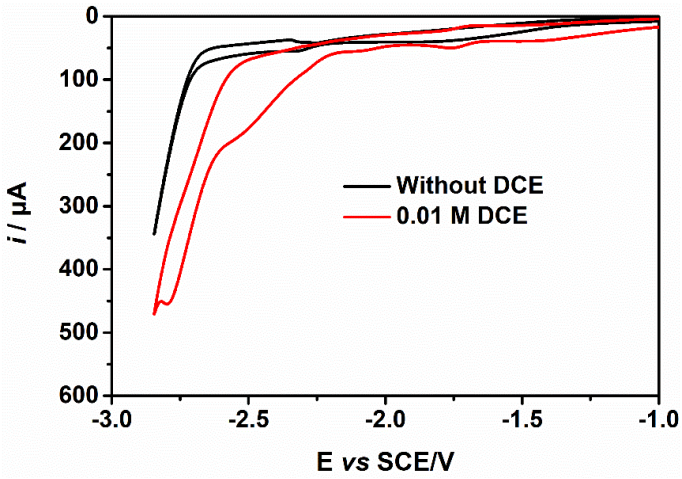

Figure S9. Cyclic voltammetry curves of Fe−N_x−Cn−800 with and without 0.01 M DCE, which acquired in the DMF solution with 0.1 M *n*-Bu_4NBF_4 using the glassy carbon working electrode with the catalyst load of 0.2 mg cm^{-2}.

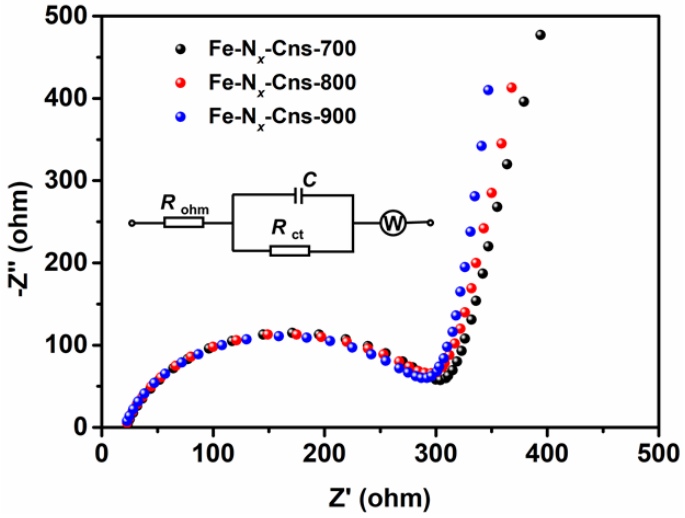

Figure S10. Electrochemical impedance spectroscopic (EIS) Nyquist plots of Fe−N$_x$−Cns, the inset is the equivalent circuit.

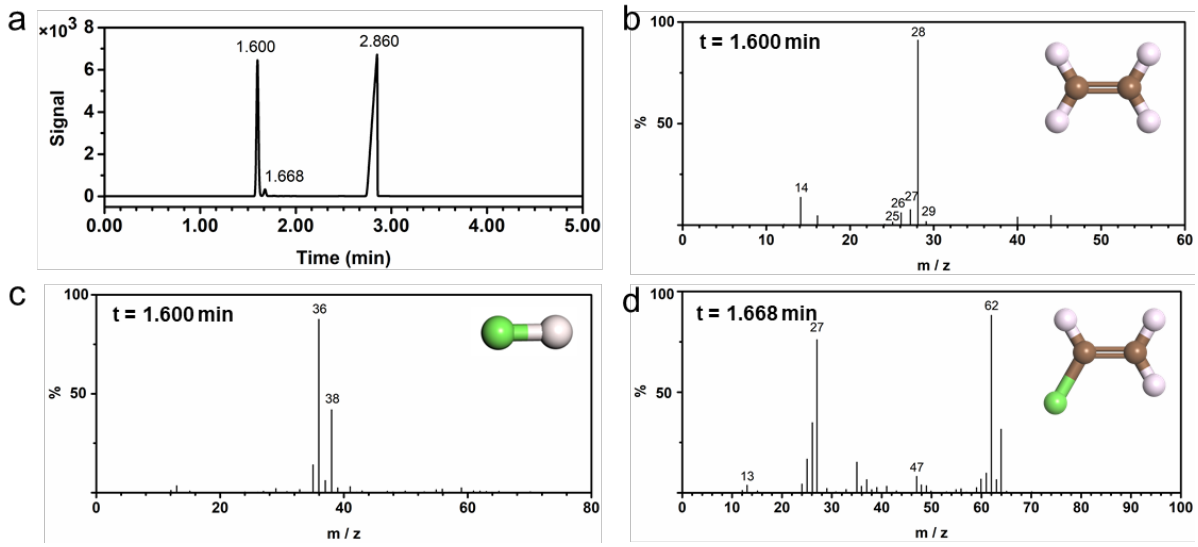

Figure S11. GC-MS spectra of the final gas products: (a) total ions chromatogram, where the peak at 1.600 min is assigned to ethylene and hydrogen chloride, the peak at 1.668 is vinyl chloride, and the peak at 2.860 is 1,2-dichloroethane; and mass spectra of (b) ethylene, (c) hydrogen chloride, and (d) vinyl chloride.

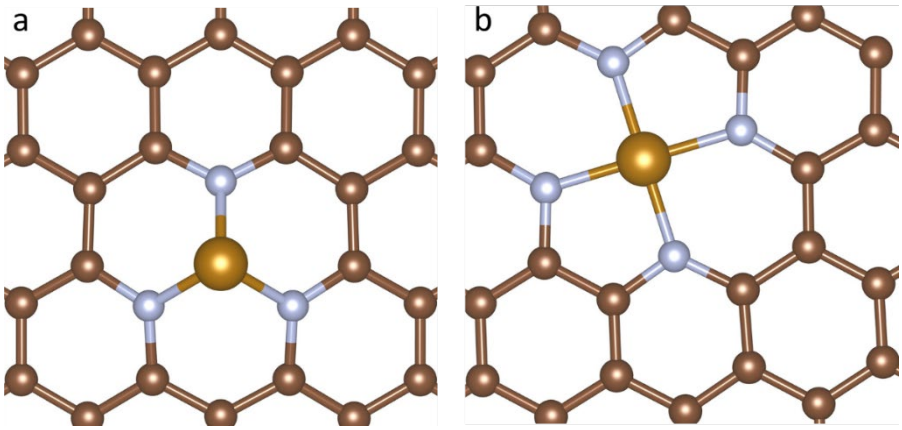

Figure S12. Geometry structure of a) Fe−N_3, and b) Fe−N_4 sites at the atomic level from the first-principle.

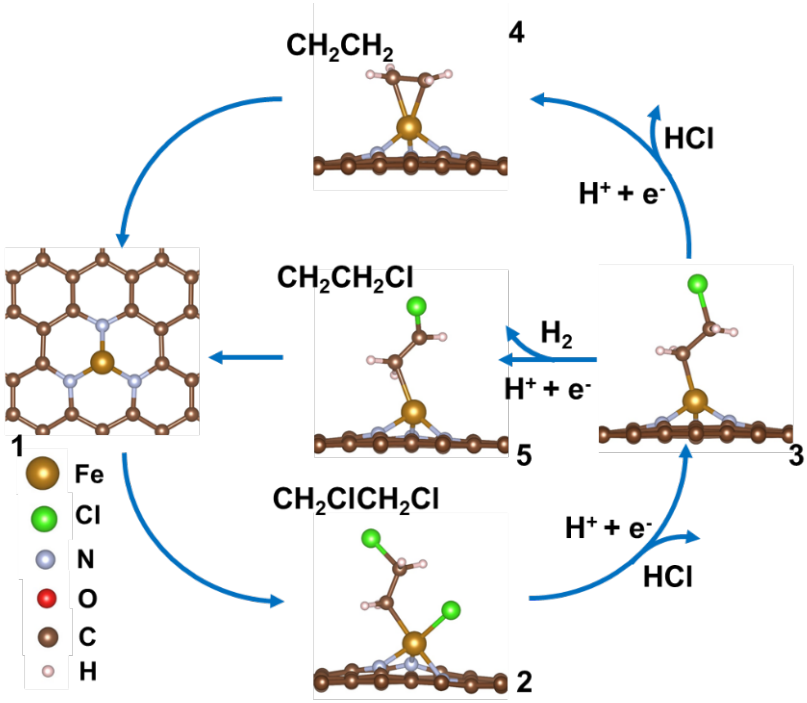

Figure S13. Illustration of the DCE dechlorination pathway on Fe−N_3 site.

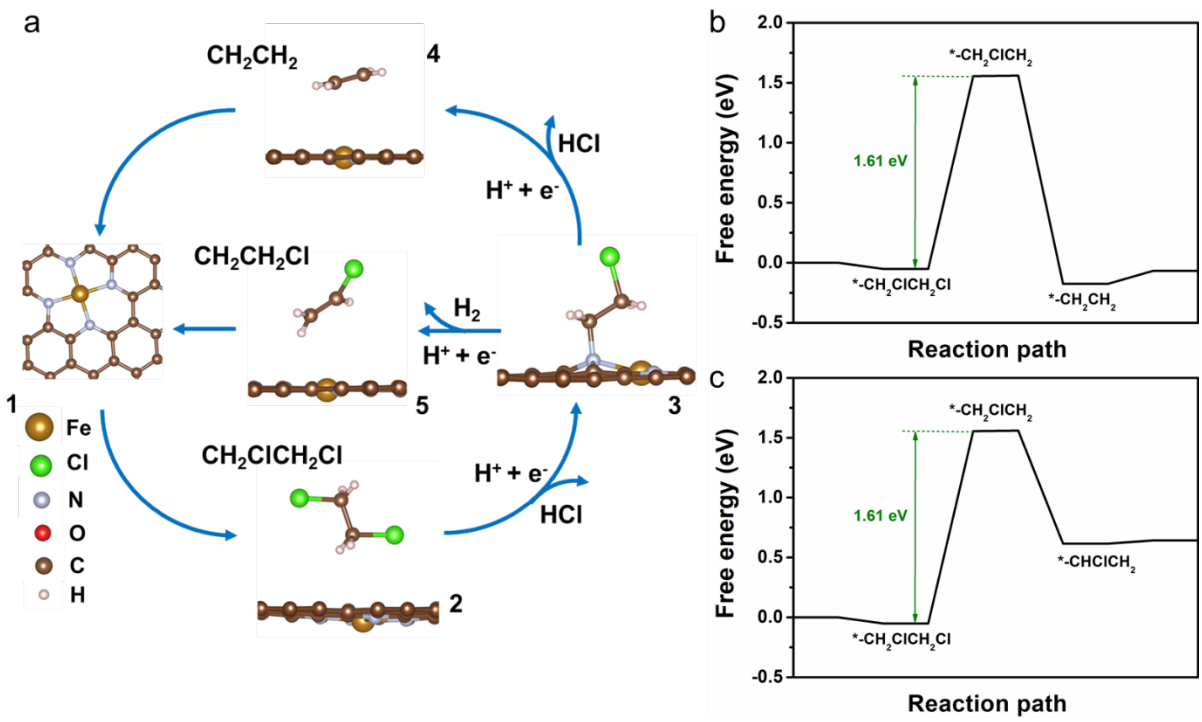

Figure S14. a) Illustration of the DCE dechlorination pathway on N site of Fe−N_4 structure. b, c) The energy profile for DCE dechlorination to b) ethylene and c) vinyl chloride on N site of Fe−N_4 structure.

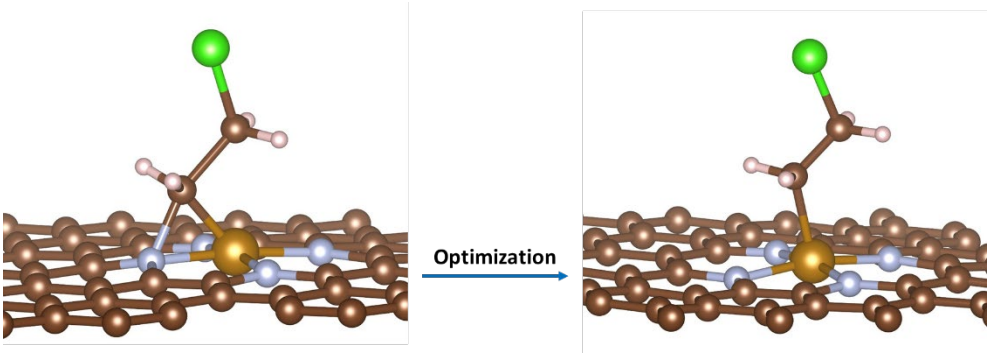

Figure S15. Geometry structure of N-C-Fe model before and after optimization.

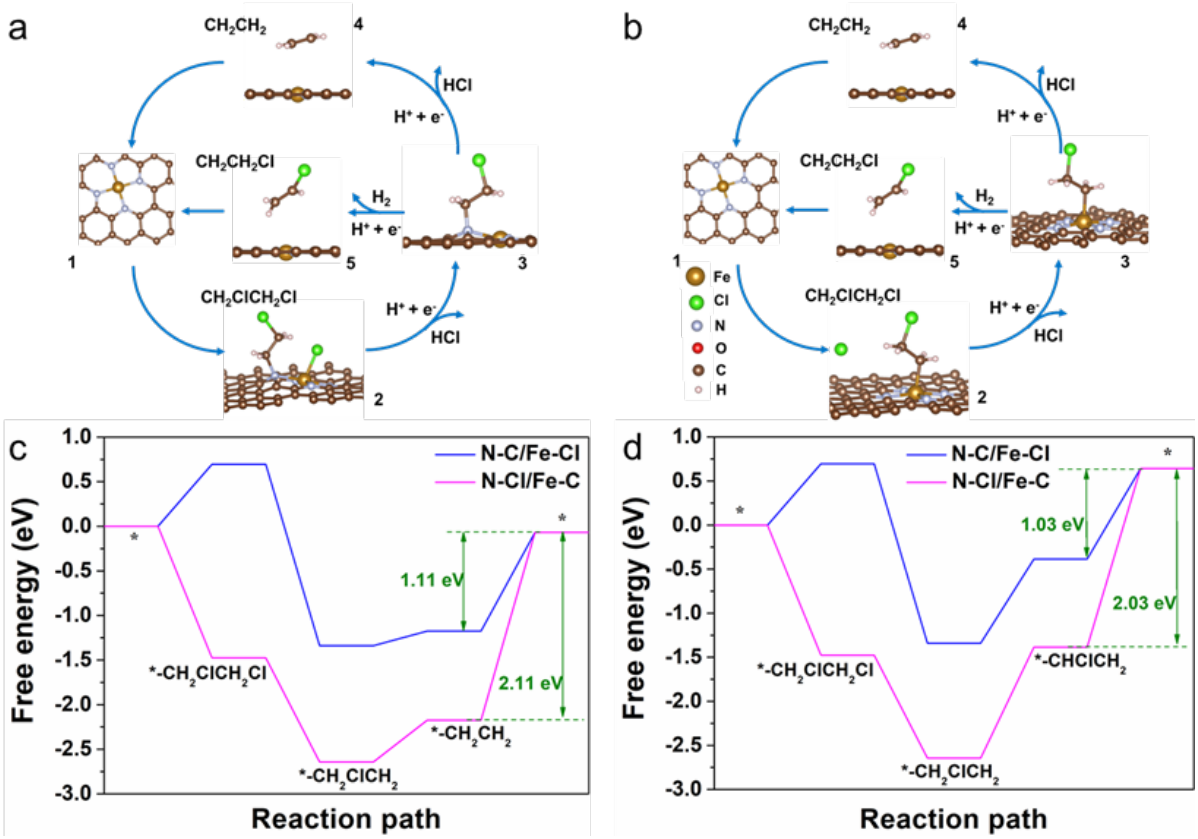

Figure S16. a, b) Illustration of the DCE dechlorination pathway on the models of a) N−C/Fe−Cl, and b) N−Cl/Fe−C. c, d) The energy profile for dechlorination of DCE into c) ethylene and d) vinyl chloride on the models of N−C/Fe−Cl and N−Cl/Fe−C.

Table S1. Pore structure parameters of Fe−N_x−Cns.

Samples	S_{BET} (m^2/g)	S_{Micro} (m^2/g)	V_T (cm^3/g)	V_{Micro} (cm^3/g)	V_{Micro}/ V_T	Average Pore Size (nm)
Fe−N_x−Cns−700	638	521	0.437	0.241	0.55	2.83
Fe−N_x−Cns−800	459	325	0.426	0.151	0.35	3.70
Fe−N_x−Cns−900	296	141	0.322	0.075	0.23	4.34

Table S2. Equivalent circuit model corresponding to the Nyquist plots of Fe−N_x−Cns.

Samples	R_{ohm} (Ω cm^{-2})	R_{ct} (Ω cm^{-2})	C (F cm^{-2})	W (S*Sec^5 cm^{-2})
Fe−N_x−Cns−700	23.8 ± 0.5	318.8 ± 1.67	0.9369 ± 0.003	3.483 ± 0.005
Fe−N_x−Cns−800	22.6 ± 0.4	316.8 ± 3.02	0.9349 ± 0.005	2.796 ± 0.004
Fe−N_x−Cns−900	22.0 ± 0.6	306.8 ± 2.23	0.9445 ± 0.004	2.697 ± 0.002

Table S3. EXAFS fitting results of Fe in Fe−N_x−Cns−800 and FePc.

Sample	Path	Coordination number	R (Å)	σ^2 (10^{-3} $Å^2$)	R-factor
Fe−N_x−Cns−800	Fe−N (O)	5.70 ± 0.32	2.01 ± 0.01	10.02	0.005
FePc	Fe−N	4.08 ± 0.42	1.93 ± 0.03	4.03	0.018

R is the distance between absorber and backscatter atoms, σ^2 is Debye-Waller factor to account for both thermal and structural disorders, *R* factor indicates the goodness of the fit.